



Subscriber access provided by Oregon State University

Physical Insights into Light Interacting with Matter

Photoinduced Charge Transfer and Bimetallic Bond Dissociation of a Bi-W Complex in Solution

Sean A. Boulanger, Liangdong Zhu, Longteng Tang, Sumit Saha, Douglas A Keszler, and Chong Fang J. Phys. Chem. Lett., Just Accepted Manuscript • DOI: 10.1021/acs.jpclett.0c02380 • Publication Date (Web): 20 Aug 2020 Downloaded from pubs.acs.org on August 20, 2020

Just Accepted

"Just Accepted" manuscripts have been peer-reviewed and accepted for publication. They are posted online prior to technical editing, formatting for publication and author proofing. The American Chemical Society provides "Just Accepted" as a service to the research community to expedite the dissemination of scientific material as soon as possible after acceptance. "Just Accepted" manuscripts appear in full in PDF format accompanied by an HTML abstract. "Just Accepted" manuscripts have been fully peer reviewed, but should not be considered the official version of record. They are citable by the Digital Object Identifier (DOI®). "Just Accepted" is an optional service offered to authors. Therefore, the "Just Accepted" Web site may not include all articles that will be published in the journal. After a manuscript is technically edited and formatted, it will be removed from the "Just Accepted" Web site and published as an ASAP article. Note that technical editing may introduce minor changes to the manuscript text and/or graphics which could affect content, and all legal disclaimers and ethical guidelines that apply to the journal pertain. ACS cannot be held responsible for errors or consequences arising from the use of information contained in these "Just Accepted" manuscripts.

Manuscript for J. Phys. Chem. Lett. (2020)

Photoinduced Charge Transfer and Bimetallic Bond Dissociation of a Bi–W Complex in Solution

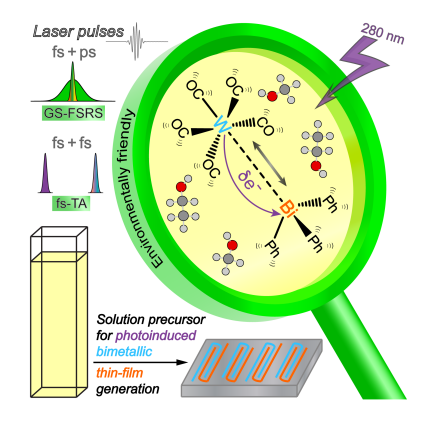
Sean A. Boulanger, Liangdong Zhu, Longteng Tang, Sumit Saha, † Douglas A. Keszler, and Chong Fang*

Department of Chemistry, Oregon State University, 153 Gilbert Hall, Corvallis, Oregon 97331-4003, United States

^{*}To whom correspondence should be addressed. Email: Chong.Fang@oregonstate.edu

ABSTRACT. Organometallic complexes including metal carbonyls have been widely utilized in academic and industrial settings for purposes ranging from teaching basic catalytic reactions to developing state-of-the-art electronic circuits. Characterization of these materials can be obtained via steady-state measurements; however, the intermediate photochemical events remain unclear, hindering effective and rational molecular engineering methods for new materials. We employed femtosecond transient absorption (fs-TA) and ground-state femtosecond stimulated Raman spectroscopy (FSRS) on triphenylbismuth-tungsten pentacarbonyl complex, a solution precursor for bimetallic oxide thin films. Upon 280 nm excitation into a charge-transfer band, an ultrafast bimetallic bond dissociation occurs within ~140 fs. The sub-picosecond non-diffusive solvation events are followed by ~10 ps (15 ps) methanol (ethanol) complexation of the nascent tungsten pentacarbonyl intermediate, which mainly undergoes vibrational relaxation after crossing into a hot ground state. The *trans* ligand to axial CO is revealed to play a key role in the electronic and vibrational structure and dynamics of the complex. These findings could power rational design of bimetallic and functional solution precursors for the light-driven nanopatterning of thin films.

TOC GRAPHIC



KEYWORDS: bimetallic complex, photochemistry, solution precursor, ultrafast bond cleavage, vibrational relaxation, light-driven nanowrite

The study of kinetic versus thermodynamic stability of organometallic transition metal compounds gained popularity in the early 1970s when Wilkinson and Lappert examined the properties of metal-carbon σ bonds. ¹⁻³ Such fundamental knowledge provided insights into the metal-carbon and metal-hydrogen bond enthalpies for revealing catalytic reaction mechanisms. For example, tungsten was found to have higher thermal and atmospheric stability in a metal complex than other Group 6 transition metals, thus often used in model systems such as tungsten hexacarbonyl, W(CO)₆, in studying ligand substitution kinetics in photosubstitution chemistry. This information is of vital importance in synthetic and industrial applications, including metal oxide thin film production, catalysis for the olefin isomerization and oligomerization, and related processes. ⁴⁻⁸ Meanwhile, bismuth oxide thin films have intriguing properties including a significant band gap and high photoconductivity. ⁹ For other bimetallic thin films beyond W/Bi, recent examples include a discrete Pt/Pd ultra-thin film-based hydrogen (H₂) sensor with fast response-recovery time, ¹⁰ and Pd/Ni thin films prepared by an electrodeposition method that have become potent electrocatalysts to oxidize methanol and ethanol in alkaline media. ¹¹

Inorganic thin-film device manufacturing requires high purity, homogeneous layering, and particles on the tens of nanometers (nm) scale to achieve suitable electronic and optical properties. Current top-down fabrication methods in nanoelectronics and quantum devices involve conventional photolithography and the more advanced electron beam-induced deposition methods to achieve higher spatial resolution.^{12,13} From the bottom up, starting from small nanocluster building blocks with electron beam and/or extreme UV exposures, organometallic precursors can now be used to produce the highest resolution structures (e.g., single-digit-nm patterning).¹⁴ However, the molecular dynamics behind such light-driven chemical reactions remain largely unknown and lag behind the engineering advances and burgeoning applications.

Photochemical reaction mechanisms involve the Franck-Condon (FC) region, metal-to-ligand charge transfer (MLCT), solvation effects, and energy relaxation, which can be elucidated by ultrafast electronic and vibrational spectroscopic methods. 6,15-18 The Group 6 hexacarbonyls, specifically W(CO)₆, have been studied in both gas phase^{7,19,20} and condensed phase; ^{6,8,15,16,21,22} however, mechanistic details of the photochemistry of heterometallic, carbonyl-containing compounds are relatively scarce. We previously investigated photochemical events of W(CO)₆ and triphenylbismuth (Ph₃Bi) separately in solution to determine the formation pathways of the W(CO)₅-solvent photoproduct and crystalline bismuth thin films. ^{8,23} Herein, we investigated the photochemical reaction coordinates for dissociation of the bimetallic triphenylbismuth-tungsten pentacarbonyl (Ph₃Bi-W(CO)₅, abbreviated as Bi-W) complex in solution. The Bi-W complex was synthesized and characterized by X-ray crystallography to have a rather long metal-to-metal bond.²⁴ To gain electronic and structural dynamics insights, we performed steady-state UV/Visible spectroscopy, femtosecond transient absorption (fs-TA) spectroscopy, ground-state femtosecond stimulated Raman spectroscopy (GS-FSRS), ^{25,26} and quantum calculations of three sample systems: 1 W(CO)₆ in methanol (MeOH), 2 Bi-W in MeOH, and 3 Bi-W in ethanol (EtOH) (see Figure 1a-c insets). Details on the experimental setup and computational methods can be found in the Supporting Information. The elucidation of distinct steps and reaction intermediates following UV photoexcitation provides a foundation to define the principles for designing solution precursors for deposition of photoactive films and writing ultra-high resolution nanostructures.^{27,28}

The absorption spectra before and after UV laser pump of **1-3** (Figure 1a-c) provide electronic signatures of the reactants and photoproducts. We assigned the emerging peak at 419 nm for W(CO)₆ in MeOH to the UV-light-induced formation of an irreversible W(CO)₅(OHCH₃)

photoproduct.⁸ A notable difference between the absorption spectra of W(CO)₆ and Bi–W in solution before UV excitation is the presence of a weak band at the position of the photoproduct in the Bi–W samples (Figure 1). The absence of this 419 nm band in both W(CO)₆ and Ph₃Bi in MeOH before UV excitation (Figure S1), as well as the presence of an absorption band around 420 nm for many other W(CO)₅–L species (L is the coordinating ligand),²⁹ confirm that the 419 (416) nm peak of Bi–W in MeOH (EtOH) is associated with the W(CO)₅–L complex. Moreover, the absorption cross section of the W(CO)₅–solvent complex is likely higher than that of the Bi–W complex in the visible region as reflected by an increase of the absorption band intensity.^{4,8,21}

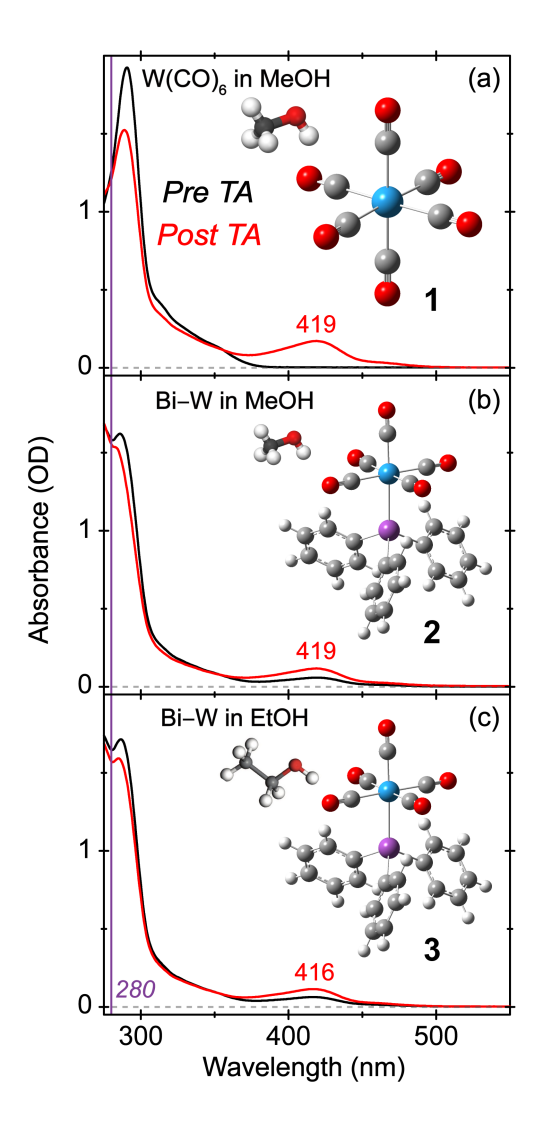


Figure 1. Chemical structures and steady-state electronic spectroscopy before (black) and after (red) UV photoexcitation of 2 mM (a) W(CO)₆ in MeOH, (b) Bi–W in MeOH, and (c) Bi–W in EtOH. The violet vertical line represents the 280 nm actinic pump for fs-TA. The ball-and-stick models for representative solute and solvent molecules depict the color-coded atoms (spheres): hydrogen (white), carbon (gray), oxygen (red), tungsten (cyan), and bismuth (magenta).

The UV absorption band near 310 nm for W(CO)₆ in MeOH was assigned to ${}^{1}A_{1g} \rightarrow {}^{1}T_{1g}$ spin-allowed ligand field transition^{16,29} with later computation-aided assignments involving some MLCT character.^{30,31} Group 6 hexacarbonyls show a blue-shifted UV excitation (~290 nm) that induces an M d $\rightarrow \pi^*$ CO charge transfer,⁷ leading to the M–CO bond dissociation, whereas, bimetallic species have a dominant localized $\sigma \rightarrow \sigma^*$ electronic transition in the UV (~230 nm) that is responsible for M–M bond dissociation^{32,33} (Figure S2). A red-shifted UV excitation of the CT band (in the FC region) in transition metal complexes can also lead to bond elongation and rapid metal-ligand dissociation^{18,32,34} in the promptly populated singlet state (S₁).^{16,20,30}

The GS-FSRS of W(CO)₅–L (Figure 2) reveals the axial ligand-dependent frequency shift of key carbonyl and phenyl ring vibrational motions (Table S1), confirming the photoinduced reaction from Bi–W to W(CO)₅(OHCH₃) in MeOH. The initial pale-yellow solution darkened after ~30 minutes of UV lamp irradiation. Longer irradiation (30–50 minutes) resulted in a brown solution with accumulation of some black powders, which raised the spectral baseline of the electronic absorption spectrum (Figure S3). We found that the black precipitate was graphitic carbon with trace amounts of crystalline bismuth.²³

The GS-FSRS spectral window from ~350 to 2300 cm⁻¹ captures three common vibrational motions of the related complexes: W–C stretch (~434 cm⁻¹), W–C=O deformation (~480 cm⁻¹), and in-plane C=O antisymmetric stretch (~2030 cm⁻¹). Symmetry reduction from the parent

octahedral W(CO)₆ to pentacarbonyl complexes accounts for the differing vibrational pattern⁸ with five major Raman peak frequency shifts (see Figure 2b and Table S1): axial W–C stretch $(470\rightarrow478~\text{cm}^{-1})$, W–C=O bending motions $(534\rightarrow572~\text{cm}^{-1})$, benzene ring C=C stretch $(1680\rightarrow1728~\text{cm}^{-1})$, in-plane four C=O antisymmetric stretch $(2137\rightarrow2145~\text{cm}^{-1})$, and five C=O symmetric stretch $(2189\rightarrow2204~\text{cm}^{-1})$. The W–C stretching mode was proposed to govern the *trans* ligand ejection,^{21,31} whereas C–W–C bending motions could facilitate an efficient internal conversion from S₁ to S₀;²⁰ however, we only imply these reaction coordinates from the equilibrated GS-FSRS data before and after UV excitation on the minutes timescale.⁸

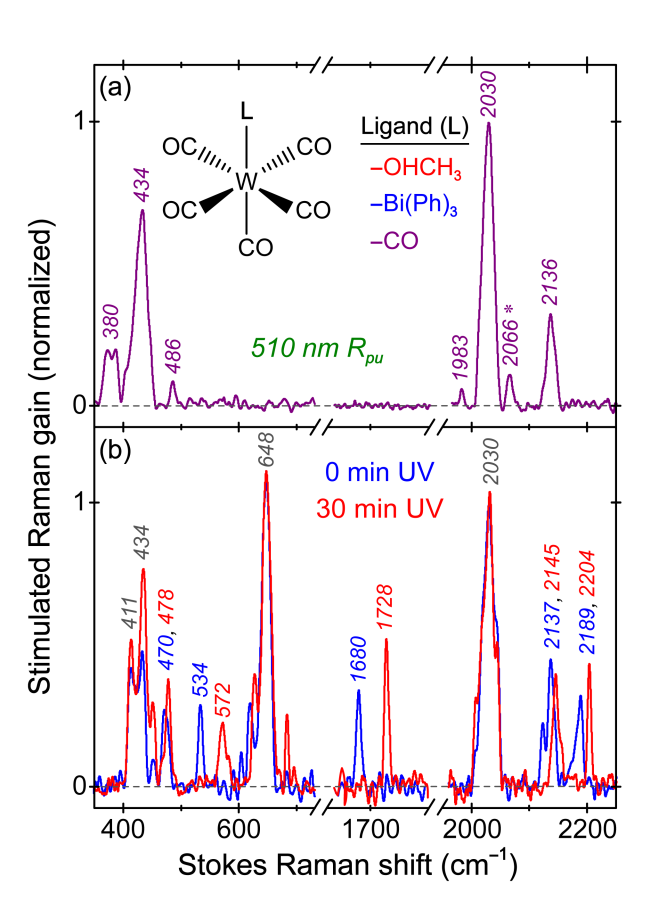


Figure 2. Normalized GS-FSRS spectra of 5 mM (a) W(CO)₆ in MeOH (purple) and (b) Bi–W in MeOH before (blue) and after (red) UV lamp irradiation at 254 nm for 30 minutes. The Raman pump was tuned to 510 nm. Mode assignments of the vibrational peaks labeled are listed

in Table S1. The molecular complex is displayed in the (a) inset with various ligands (L) color-coded according to their individual spectrum. The asterisk by the 2066 cm⁻¹ peak denotes a small shoulder band that could be due to a minor population in solution or anharmonic terms.

The axial W–C and collective C=O stretching modes blueshift upon photoproduct formation, likely due to the increased π-backbonding from W to the axial CO that is affected by the electron-donating ability of the *trans* ligand.³⁵ Since the *trans* ligand donor strength increases from CO, Bi(Ph)₃ to OHCH₃, we performed density functional theory (DFT) geometric optimization and frequency calculations that yield a strong correlation between the v(W–CO) vs. v(C=O) frequencies and W–CO vs. C=O bond lengths (Figure S4). The negative correlation between these two adjacent axial bonds arises from an interplay between σ-bonding and π-backbonding for W–L and W–CO. In Figure 2b, the shared ~2030 cm⁻¹ band is a triplet that is not easily resolved; however, the calculated trend largely agrees with experimental results. The W–C stretching mode likely involved in *trans* CO and Bi(Ph)₃ ligand ejection is a result of asymmetric stretching motions, particularly in the axial CO, which releases translational energy along the reaction coordinate.^{21,31} The pronounced axial C=O stretching motions at 2030 cm⁻¹ with resonance Raman enhancement in Figure 2 corroborate the vibronic coupling effect.^{17,21,36,37}

The benzene ring deformation at ~648 cm⁻¹ exhibits a small shoulder on the red side which may affect the peak frequency determination. Calculations predict a slight frequency redshift from the reactant to photoproduct (Table S1), consistent with a lengthening of the Bi–C bond (2.19 to 2.23 Å).³⁸ Notably, the concomitant blueshift of the benzene ring C=C stretching mode in GS-FSRS (1680→1728 cm⁻¹ in Figure 2b) indicates an increase of electron density on the phenyl groups following W–Bi bond dissociation,³⁹ implying a CT process (see below). However, the calculated C=C bond lengths are ~1.4 Å in both the bound (Table S2) and unbound

Bi(Ph)₃ ligand, pointing to the effect of intermolecular interactions that may not be accurately modeled in solution (see Supporting Information). The Bi–C stretch (~206 cm⁻¹) and bimetallic stretch (<200 cm⁻¹) were not observed since they occur at lower frequencies than the current detection window.^{23,40}

Important information about the photoinduced reactants and products was obtained via the steady-state electronic and GS-FSRS data; however, there remains a plethora of knowledge in bridging the gap between these two species. To delineate the excited-state reaction coordinates, we strategically tuned our actinic pump to 280 nm to track the transient dynamics via fs-TA. The pump is deemed appropriate since the ~285 nm absorption band decreases more in intensity for $W(CO)_6$ ($d\rightarrow\pi^*$ CT) than that for Bi–W (Figure 1). The emergence of a 419 nm band after UV excitation of $W(CO)_6$ (black to red trace in Figure 1a) shows the loss of a CO ligand in MeOH solution. G-8,16,21 In contrast, the actinic pump into a CT band (Figure S2) could efficiently break the W–Bi bond ("weakest" link) without W–CO dissociation of the tungsten pentacarbonyl species, as supported by the aforementioned steady-state absorption and GS-FSRS results. The steady-state absorption and GS-FSRS results.

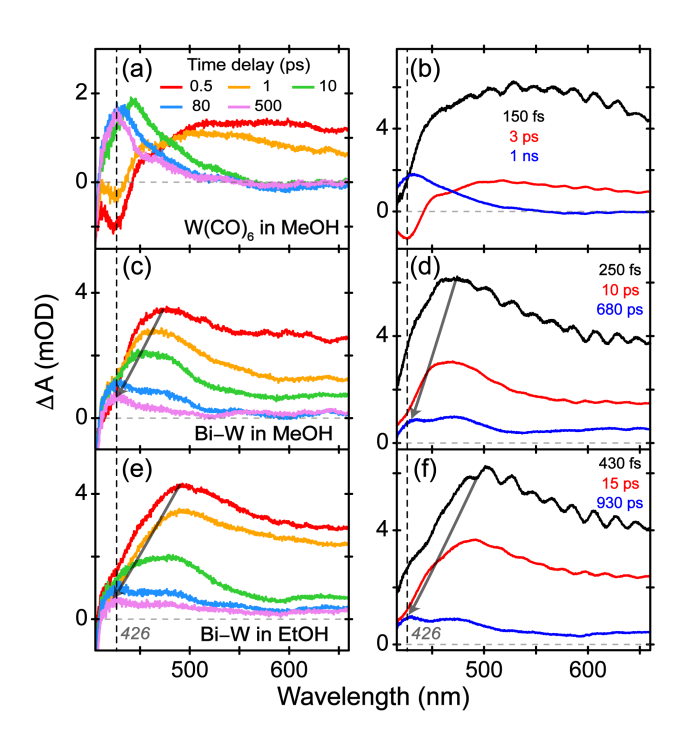


Figure 3. Transient electronic dynamics of W(CO)₆ and Bi–W complexes in solution. Fs-TA spectra at selected time points for 2 mM (a) W(CO)₆ in MeOH, (c) Bi–W in MeOH, and (e) Bi–W in EtOH track the excited-state events after UV photoexcitation, with global analysis results in (b), (d), and (f), respectively. The evolution-associated difference spectra consist of three major components (black, red, and blue). The black dashed vertical line denotes the W(CO)₅–solvent photoproduct at late times and gray arrows highlight the TA peak wavelength blueshift.

The electronic excited-state dynamics of Group 6 hexacarbonyls upon UV excitation exhibit characteristic TA signatures. ^{15,16,18} Herein, the 280 nm excitation of W(CO)₆ in MeOH (Figure 3a) leads to a photochemical reaction that occurs primarily in three stages: ultrafast W–CO bond dissociation and relaxation, solvation of the nascent W(CO)₅ to form W(CO)₅(OHCH₃), and further vibrational cooling. ^{6-8,16,21,22,33} The probe-dependent dynamics at 480, 440, and 410 nm (Figure S5b-d) share a similar initial decay time constant (120–180 fs), ^{8,16,21} in conjunction with the instrument response function of ~140 fs, largely matching the reported time of ca. 100–300 fs for ejection of the first CO ligand from W(CO)₆ in solution. ^{6,21} Both the rise and second decay components lengthen as the probe shifts toward the photoproduct species at ~426 nm, denoting a blueshift of the dominant excited-state absorption (ESA) band. ⁸ The intermediate rise time constants are 1.5, 2.5, and 8.2 ps at 480, 440, and 410 nm probe, respectively, in correlation with ultrafast solvent motions (see below). The second decay time constant (6 and 15 ps with 480 and 440 nm probe) becomes much longer (1.3 ns) with 410 nm probe due to the overlap with a hot-GS absorption band, which occurs to the red side of the ground-state bleaching (GSB) band. ³⁷

Upon W–CO photodissociation, the nascent $W(CO)_5$ species may rapidly reach the S_0 state by relaxation through a Jahn-Teller-induced conical intersection (solute fragment interconversion or isomerization), reducing the GSB signal strength. 6,20,41 Meanwhile, geminate recombination of

the unsaturated W(CO)₅ with a CO trapped in the solvent cage is a competing pathway with initial solvation events;²¹ however, it was estimated from fs-IR studies of W(CO)₆ that geminate recombination of CO was ~15% and 21% in heptane and dodecane, respectively, on the ultrafast timescale of ~150 fs.⁶ Since high solvent viscosity hinders CO motions while relative viscosities increase from heptane, methanol, ethanol to dodecane, we estimate the geminate recombination in MeOH and EtOH to be <20%.⁴² Upon escaping the FC region to undergo solvent complexation, the $S_1 \rightarrow S_0$ internal conversion of nascent (CO)₅W–solvent species could be aided by either the C–W–C bending motions or ligand-to-W back CT, inducing a facile redistribution of the W d-orbital electrons to resemble the ground-state configuration on the ps timescale.^{17,20}

To complement the triexponential least-squares fits of the integrated peak intensity dynamics, global analysis of the fs-TA spectra using Glotaran⁴³ yields the evolution-associated difference spectra (EADS) with a sequential kinetic model and three time constants: ~150 fs attributed to an initial relaxation, 3 ps attributed to the MeOH complexation of the nascent W(CO)₅, and 1 ns attributed to vibrational relaxation/cooling of the hot-GS species. The 150 fs lifetime matches the mostly conserved initial decay across the spectral detection window, likely involving some ultrafast geminate recombination events (see above).⁶ The intermediate 3 ps component matches literature for MeOH complexation in Group 6 pentacarbonyls with 440–480 nm probe, ^{15,21} and with a bluer probe at 410 nm the pertinent time constant increases to 8.2 ps, largely matching the longitudinal relaxation time of MeOH (~9 ps) within the first solvation shell of the vibrationally hot W(CO)₅ (i.e., a local phenomenon). ^{16,21,22,44-46} A more quantitative assignment is hindered by the inhomogeneity of reactive species, overlap with the hot-GS absorption peak, and other competing pathways in solution. Interestingly, a discernible negative peak at ~426 nm (Figure 3b, red trace) indicates that solvent coordination to hot W(CO)₅ occurs in S₁ and a stimulated

emission band could coincide with the S_1 – S_0 energy gap of the W(CO)₅–solvent species as its electronic absorption band peaks at 419 nm in MeOH (Figure 1a, see Supporting Information for related discussions on some set-dependent accumulation of pentacarbonyl species). We note that such a transient negative feature was not observed with 267 or 308 nm excitation.^{8,21}

The much longer 1 ns decay component is consistent with that retrieved from the probedependent dynamics at 410 nm (Figure S5d). The lengthened time constants (6 ps, 15 ps to 1.3 ns) across probe wavelengths of 480, 440 to 410 nm reveal an ESA band blueshift that reflects the photoproduct formation and energy dissipation by continuous solvation.⁸ Since fs-TA tracks transient electronic features of the molecule without vibrational information, we surmise that CO stretching motions contribute to the hot-GS relaxation of this non-fluorescent molecule on the basis of prominent CO vibrational motions in GS-FSRS (Figure 2) and previous literature.^{6,21,36}

Using W(CO)₆ as the control, we employed fs-TA to dissect the electronic dynamics of the Bi–W complex in MeOH and EtOH after the fs laser pump at 280 nm. The initial intensity decay and peak blueshift indicate an already-dissociated complex with a broad ESA band (Figure 3c,e), which is narrower than that for W(CO)₆ (see Figure 3a) due to the dissociated yet adjacent ligand since the much bulkier Ph₃Bi hinders W(CO)₅ motions. In consequence, the nascent W(CO)₅ species can sample less phase space on ultrafast timescales (see below), hence the reduced ESA bandwidth.³⁷ A more dramatic spectral change (from red, orange to green trace in Figure 3c,e) would be expected if the bond dissociation occurred on the sub-ps to ps timescales.^{8,18,21} Also, bismuthine ligands have poor coordinating properties and low basicity, while the ~2.83 Å Bi–W bond is much longer and more photolabile than the ~2.05 Å W–CO bond in the W(CO)₅ moiety, implying a weaker bond between two central metal atoms.^{19,24,47} Upon UV excitation at 280 nm of Bi–W (see the electronic absorption spectrum in MeOH from time-dependent DFT (TD-DFT)

calculations, Figure S2), the major contributor is a HOMO \rightarrow LUMO+1 transition that involves clear CT from the donor to acceptor moiety (Figure 4), ^{34,48} wherein the nondissociating equatorial CO groups and *trans* CO group lose electron density while the Bi *p*-orbital and triple phenyl rings accept the shifting electron density. This CT process makes a dissociative excited-state potential energy surface^{21,30} that leads to swift elongation of the already long (2.83 Å) bimetallic bond, promoting a rapid bond dissociation following the actinic UV excitation.³⁴

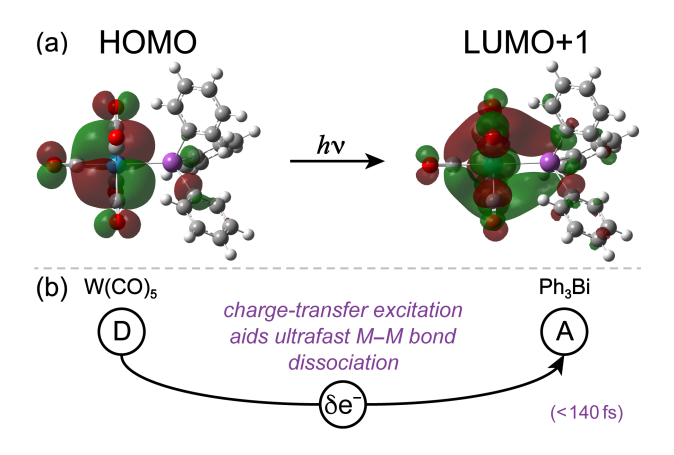


Figure 4. Quantum calculations imply the nature of electronic excitation. (a) Frontier molecular orbitals of the HOMO and LUMO+1 electron density distribution of Bi–W in MeOH from TD-DFT energy calculations at the optimized geometry of the electronic ground state. Red and green shades represent the positive and negative phases of the pertinent MOs (isovalue of 0.02 *e*/Å³). (b) Ultrafast bimetallic bond dissociation is accompanied by charge transfer between the W(CO)₅ donor (D) and the Ph₃Bi acceptor (A) moieties upon UV photoexcitation.

The Bi–W complexes in MeOH (EtOH) share similar time constants, 120–150 fs (100–150 fs), across various probe wavelengths at 540, 480, and 440 nm (Figure S5a-c) for the initial decay. The second and third decay components lengthen as the probe wavelength approaches the photoproduct at 426 nm, reminiscent of the aforementioned ESA peak blueshift. The associated

Page 14 of 33

time constants for Bi-W in MeOH (EtOH) are 5, 10, and 15 ps (11, 16, and 25 ps) and 300 ps, 640 ps, and 1.5 ns (650 ps, 1.3 ns, and 2.5 ns) at 540, 480, 440 nm probe wavelengths, respectively. The W(CO)₅ intermediate can either take $C_{4\nu}$ (square pyramid) or D_{3h} (trigonal bipyramid) symmetry in the excited state, ^{7,49} but the long-lived ESA band near 480 nm is likely due to $C_{4\nu}$ W(CO)₅ weakly coordinated with the displaced Ph₃Bi ligand or a solvent molecule since D_{3h} W(CO)₅ species typically absorb at lower energy and have a triplet ground state. ^{29,49,50} Since the formation of the complexed W(CO)₅–L species via the D_{3h} pathway was reported to be faster than the C_{4v} pathway on the few ps timescale in solution, 51 the apparently broader ESA band after photoexcitation of W(CO)₆ (black trace in Figure 3b) than that of Bi–W (black trace in Figure 3d) in the same solvent (MeOH) could be due to a larger percentage of D_{3h} species after ejection of one CO from W(CO)₆, particularly with the 280 nm laser excitation that has more excess energy than the 310 or 289 nm pump used. 21,36 Using global analysis to retrieve the underlying species of UV-irradiated Bi-W in MeOH (Figure 3d) and EtOH (Figure 3f), the EADS model yields a three-stage reaction (Scheme 1) after a <140 fs bimetallic bond dissociation upon UV excitation into a CT state: 250 fs (430 fs) FC relaxation, 10 ps (15 ps) local solvation, and 680 ps (930 ps) further vibrational relaxation. These characteristic time constants better represent the photoinduced molecular dynamics since global analysis accounts for all species present in the sample and covers the broadband detection spectral window.

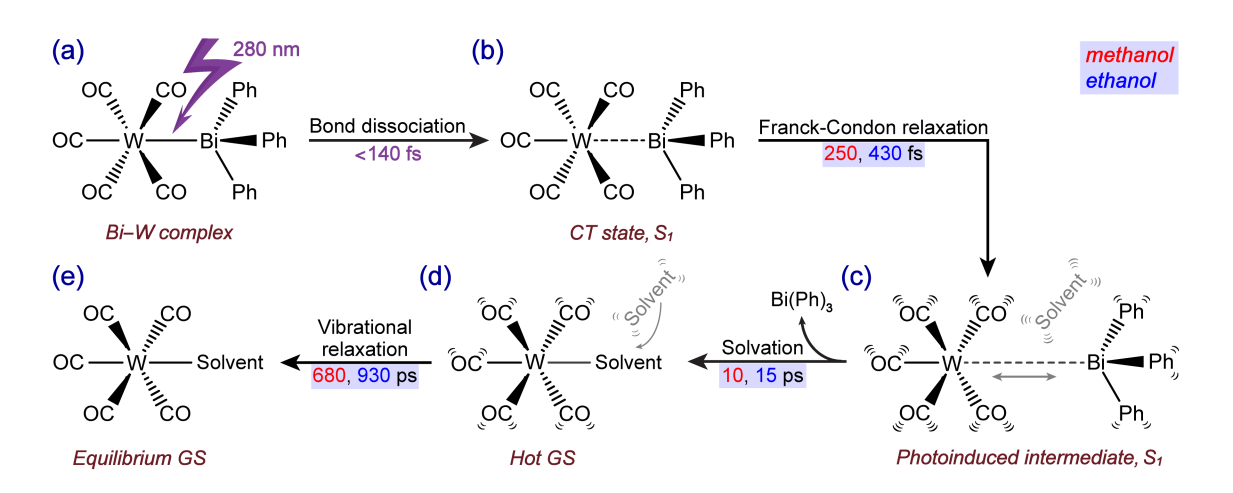
Notably, the ultrafast bimetallic bond dissociation within the instrument response function (Supporting Information) is consistent with the stepwise dissociative electron transfer (DET) theory, wherein simultaneous electron transfer and bond dissociation occur⁵² with a dominant effect in the solvent reorganization energy term, which allows for distinction between inertial and diffusive solvent molecular motions. ^{47,52-54} Non-diffusive hindered solvent rotation in MeOH

(EtOH) was reported to be 210 fs (290 fs), ^{18,55} closely matching our experimental values of 250 fs (430 fs) in MeOH (EtOH). A similar heavy-atom displacement was observed during the initial separation between Br and CHBr₂ moieties after the 268 nm laser-induced C-Br bond fission of bromoform (CHBr₃) in gas phase, which occurs after ~300 fs.⁵⁶ Next, the retrieved 10 ps (15 ps) component largely matches the solvent longitudinal relaxation time within the first solvation shell. 44-46,55,57 To rationalize the interesting observation that the ESA peak blueshifts from ca. 472→464 nm and 503→484 nm for Bi–W in MeOH and EtOH as shown by the black→red trace in Figure 3d and 3f, respectively, a CT process is likely present within the nascent excited-state W(CO)₅-solvent species following the initial CT excitation of the Bi-W complex, which leads to a solvatochromic effect. 37,58,59 Due to the higher polarity of methanol (the normalized $E_T^N =$ 0.762) than ethanol $(E_T^N = 0.654)^{58,60}$ the dominant $C_{4\nu}$ species with an electric dipole moment that decreases from $S_1 \rightarrow S_n$ ($n \ge 2$) would have a bluer ESA band maximum in methanol than that in ethanol. In contrast, the D_{3h} species that absorb at the redder region (>560 nm) have a net zero dipole moment and do not contribute to the observed ESA peak blueshift (Figure 3), while the adjacent Ph₃Bi ligand after ultrafast dissociation hinders conformational motions of the W(CO)₅ moiety including pseudorotation.²⁰

Further separation between the two originally bonded central metals (W and Bi, along with their ligands) involves intermolecular diffusion on the ps to ns timescale, longer than Debye relaxation time of the solvent (e.g., ~50 ps of MeOH and 200 ps of EtOH at room temperature) for the long-range H-bond rearrangement (a bulk property). Such events mainly occur in the electronic ground state as reflected by the long-lived last components of Bi–W complex in MeOH and EtOH with the hot-GS absorption band (blue traces in Figure 3d,f). Experimentally, a clear transition from one broad ESA band (red traces in Figure 3d,f) to two discernible bands

(blue traces in Figure 3d,f, with the rising ~426 nm peak) substantiates the emergence of hot GS species. We thus conclude that the Bi–W bond scission is followed by three distinct reaction steps in solution which effectively dissipates the photoexcitation energy: non-diffusive hindered solvent rotation with concurrent displacement between the CT donor and acceptor moieties (Figure 4b) to assist initial W(CO)₅ relaxation out of the FC region, W(CO)₅–solvent photoproduct formation and passage through a conical intersection, and hot-GS relaxation of the W(CO)₅–solvent complex.

Scheme 1. Photochemical reaction mechanism of Bi–W in solution. Characteristic time constants are listed by major steps converting the reactant (a) via intermediates to the product (e).



Besides real-time tracking of the W(CO)₅–solvent photoproduct, the photochemistry of the Ph₃Bi ligand cannot be neglected despite its relative inertness and lack of vacant site for solvent coordination. Not only is Ph₃Bi a much more bulky and less mobile ligand than CO, hence inducing significant steric hindrance for the initial solvation events and W(CO)₅–solvent interactions, prolonged UV excitation of the photolabile Bi–C bonds in organic solvents may also lead to graphitic carbon and crystalline bismuth thin film formation.²³ To mitigate the light-induced gradual cloudiness of sample solution during fs-TA experiments, we used a miniature

stir bar and also vertically moved the sample to ensure that the incident laser pulses probe a fresh and transparent sample region.

Unlike W(CO)₆ and similar systems, geminate recombination between the nascent W(CO)₅ intermediate and the photodissociated Ph₃Bi ligand is not expected due to the poor coordinating properties of bismuthine ligands.^{24,47} Moreover, solvation of W(CO)₅ should outcompete geminate recombination by hindrance of a symmetry-induced conical intersection, leading to internal conversion away from the FC region via either C–W–C bending motions or ligand-to-W back CT.^{6,17,20,41,62-64} Later in Scheme 1, the hot-GS vibrational relaxation via high-frequency CO stretching motions occurs on a similar hundreds-of-ps timescale as reported for W(CO)₆ and other Group 6 metal carbonyls.^{22,36} However, this process occurs faster in Bi–W than W(CO)₆ (see Figure 3), likely due to more effective energy dissipation via collisions between the W(CO)₅–solvent photoproduct and the nearby bulky Ph₃Bi ligand, nascent crystalline bismuth, and graphitic carbon in solution in returning to the equilibrated ground state.²³ The associated time constant is slightly larger for Bi–W in EtOH (930 ps) than in MeOH (680 ps), in accord with the higher viscosity of EtOH as well as thermal equilibration in both solvents.^{33,61}

In summary, we implemented the steady-state electronic spectroscopy, broadband fs-TA, GS-FSRS, and quantum calculations to elucidate the photochemical reaction coordinates of a prototypical Bi–W complex in solution. The 280 nm photoexcitation induces an ultrafast charge transfer between the W(CO)₅ and Ph₃Bi moieties that results in an effective bimetallic bond scission within ~140 fs. The non-diffusive solvent motions and displacement between the W(CO)₅ intermediate and Ph₃Bi species facilitate rapid relaxation from FC region so solvent coordination/complexation can occur at the vacant site of the reactive W(CO)₅ intermediate species. Internal conversion through intramolecular vibrations and/or ligand-to-W back CT^{17,64}

bring the photoproduct to a hot ground state wherein CO stretches (prominent in GS-FSRS) dissipate the remaining energy on the hundreds-of-ps timescale. The W-C stretching mode responsible for the trans CO and Ph₃Bi ligand ejection affects the π -backbonding from W to the axial CO as a result of charge redistribution, which was tracked by the frequency blueshift of the axial W-C and benzene ring C=C stretching modes from reactant to photoproduct. We integrated our previous findings about Ph₃Bi and W(CO)₆ in solution^{8,23} as a benchmark in our current axial ligand- and solvent-dependent electronic and vibrational spectroscopies. The interwoven and correlated spectroscopic fingerprints (from the electronic to vibrational domain) have enabled us to provide deeper structural dynamics insights into organometallic photochemistry with applications toward the rational design of environmentally friendly solution precursors to achieve inexpensive and high-quality microelectronics. 23,27 Moving forward, systematic studies on the modified R₃Bi-W(CO)₅ complexes (R = electron-donating or withdrawing groups) could enhance the synergy between ultrafast CT and bond scission while minimizing geminate recombination. Such an efficient bond scission would improve the efficiency and fidelity of selective area deposition and direct patterning of metal-containing films, and the light-driven functional materials and devices in general.

ASSOCIATED CONTENT

Supporting Information. The Supporting Information is available free of charge on the ACS Publications website at http://pubs.acs.org.

Experimental materials and sample preparation, steady-state electronic and femtosecond transient absorption (fs-TA), femtosecond stimulated Raman spectroscopy (FSRS), computational methods, Figures S1-S5 on the experimental and calculated electronic and vibrational properties of the Bi–W complex in solution, Tables S1-S3 on the Raman

mode assignment and calculated vibrational frequencies and bond lengths, additional references, and the full authorship of Gaussian 09 software (PDF)

AUTHOR INFORMATION

Corresponding Author

*E-mail: Chong.Fang@oregonstate.edu. Phone: 541-737-6704.

Notes

[†]Current address: Materials Chemistry Department, CSIR – Institute of Minerals & Materials Technology, Bhubaneswar 751013, Odisha, India

The authors declare no competing financial interests.

ACKNOWLEDGMENT

This work is supported in part by the NSF CAREER grant (CHE-1455353) and MRI development grant (DMR-1920368) to C.F. We thank Cheng Chen and Taylor Krueger for helpful discussions. S.B. acknowledges the Dorothy and Ramon Barnes Graduate Fellowship (2020) at the Oregon State University Chemistry Department for funding, and the ARCS (Achievement Rewards for College Scientists) Foundation Scholarship (2017–2020).

REFERENCES

(1) Collier, M. R.; Lappert, M. F.; Truelock, M. M. μ-Methylene Transition Metal Binuclear Compounds: Complexes with Me₃SiCH₂⁻ and Related Ligands. *J. Organomet. Chem.* **1970**, *25*, C36-C38.

- (2) Wilkinson, G. The Transition Metal to Carbon Sigma Bond. *Pure Appl. Chem.* **1972**, 30, 627-636.
- (3) Davidson, P. J.; Lappert, M. F.; Pearce, R. Metal σ-Hydrocarbyls, MR_n. Stoichiometry, Structures, Stabilities, and Thermal Decomposition Pathways. *Chem. Rev.* **1976**, *76*, 219-242.
- (4) Dahlgren, R. M.; Zink, J. I. Ligand Substitution Photochemistry of Monosubstituted Derivatives of Tungsten Hexacarbonyl. *Inorg. Chem.* **1977**, *16*, 3154-3161.
- (5) Simões, J. A. M.; Beauchamp, J. L. Transition Metal-Hydrogen and Metal-Carbon Bond Strengths: The Keys to Catalysis. *Chem. Rev.* **1990**, *90*, 629-688.
- (6) Lian, T.; Bromberg, S. E.; Asplund, M. C.; Yang, H.; Harris, C. B. Femtosecond Infrared Studies of the Dissociation and Dynamics of Transition Metal Carbonyls in Solution. *J. Phys. Chem.* **1996**, *100*, 11994-12001.
- (7) Gutmann, M.; Janello, J. M.; Dickebohm, M. S.; Grossekathöfer, M.; Lindener-Roenneke, J. Ultrafast Dynamics of Transition Metal Carbonyls: Photodissociation of Cr(CO)₆ and Cr(CO)₆·(CH₃OH)_n Heteroclusters at 280 nm. *J. Phys. Chem. A* **1998**, *102*, 4138-4147.
- (8) Zhu, L.; Saha, S.; Wang, Y.; Keszler, D. A.; Fang, C. Monitoring Photochemical Reaction Pathways of Tungsten Hexacarbonyl in Solution from Femtoseconds to Minutes. *J. Phys. Chem. B* **2016**, *120*, 13161-13168.
- (9) Leontie, L.; Caraman, M.; Alexe, M.; Harnagea, C. Structural and Optical Characteristics of Bismuth Oxide Thin Films. *Surf. Sci.* **2002**, *507-510*, 480-485.
- (10) Hassan, K.; Iftekhar Uddin, A. S. M.; Chung, G.-S. Fast-Response Hydrogen Sensors based on Discrete Pt/Pd Bimetallic Ultra-Thin Films. *Sens. Actuators B* **2016**, *234*, 435-445.

- (11) Qiu, C.; Shang, R.; Xie, Y.; Bu, Y.; Li, C.; Ma, H. Electrocatalytic Activity of Bimetallic Pd–Ni Thin Films Towards the Oxidation of Methanol and Ethanol. *Mater. Chem. Phys.* **2010**, *120*, 323-330.
- (12) Ye, W.; Peña Martin, P. A.; Kumar, N.; Daly, S. R.; Rockett, A. A.; Abelson, J. R.; Girolami, G. S.; Lyding, J. W. Direct Writing of Sub-5 nm Hafnium Diboride Metallic Nanostructures. *ACS Nano* **2010**, *4*, 6818-6824.
- (13) Pillers, M.; Goss, V.; Lieberman, M. Electron-Beam Lithography and Molecular Liftoff for Directed Attachment of DNA Nanostructures on Silicon: Top-down Meets Bottom-up. *Acc. Chem. Res.* **2014**, *47*, 1759-1767.
- (14) Olynick, D.; Schwartzberg, A.; Keszler, D. A. Chapter 10 Mainstreaming inorganic metal-oxide resists for high-resolution lithography. In *Frontiers of Nanoscience*; Robinson, A., Lawson, R., Eds.; Elsevier, 2016; Vol. 11; pp 349-375.
- (15) Simon, J. D.; Xie, X. Photodissociation of Chromium Hexacarbonyl in Solution: Direct Observation of the Formation of Pentacarbonyl (methanol) chromium. *J. Phys. Chem.* **1986**, *90*, 6751-6753.
- (16) Joly, A. G.; Nelson, K. A. Femtosecond Transient Absorption Spectroscopy of Chromium Hexacarbonyl in Methanol: Observation of Initial Excited States and Carbon Monoxide Dissociation. *J. Phys. Chem.* **1989**, *93*, 2876-2878.
- (17) Franzen, S.; Kiger, L.; Poyart, C.; Martin, J.-L. Heme Photolysis Occurs by Ultrafast Excited State Metal-to-Ring Charge Transfer. *Biophys. J.* **2001**, *80*, 2372-2385.
- (18) McCusker, J. K. Femtosecond Absorption Spectroscopy of Transition Metal Charge-Transfer Complexes. *Acc. Chem. Res.* **2003**, *36*, 876-887.

- (19) Lewis, K. E.; Golden, D. M.; Smith, G. P. Organometallic Bond Dissociation Energies: Laser Pyrolysis of Iron Pentacarbonyl, Chromium Hexacarbonyl, Molybdenum Hexacarbonyl, and Tungsten Hexacarbonyl. *J. Am. Chem. Soc.* **1984**, *106*, 3905-3912.
- (20) Kosma, K.; Trushin, S. A.; Fuß, W.; Schmid, W. E.; Schneider, B. M. R. Photodissociation of Group-6 Hexacarbonyls: Observation of Coherent Oscillations in an Antisymmetric (Pseudorotation) Vibration in Mo(CO)₅ and W(CO)₅. *Phys. Chem. Chem. Phys.* **2010**, *12*, 13197-13214.
- (21) Joly, A. G.; Nelson, K. A. Metal Carbonyl Photochemistry in Organic Solvents: Femtosecond Transient Absorption and Preliminary Resonance Raman Spectroscopy. *Chem. Phys.* **1991**, *152*, 69-82.
- (22) King, J. C.; Zhang, J. Z.; Schwartz, B. J.; Harris, C. B. Vibrational Relaxation of M(CO)₆ (M=Cr, Mo, W): Effect of Metal Mass on Vibrational Cooling Dynamics and Non-Boltzmann Internal Energy Distributions. *J. Chem. Phys.* **1993**, *99*, 7595-7601.
- (23) Zhu, L.; Saha, S.; Liu, W.; Wang, Y.; Keszler, D. A.; Fang, C. Simultaneous Solution-based Generation and Characterization of Crystalline Bismuth Thin Film by Femtosecond Laser Spectroscopy. *Appl. Phys. Lett.* **2015**, *107*, 061901.
- (24) Holmes, N. J.; Levason, W.; Webster, M. Triphenylbismuthine Complexes of Group 6 Metal Carbonyls: X-ray Crystal Structures of [M(CO)₅(BiPh₃)] (M = Mo or W). *J. Organomet. Chem.* **1997**, *545-546*, 111-115.
- (25) Dietze, D. R.; Mathies, R. A. Femtosecond Stimulated Raman Spectroscopy. *ChemPhysChem* **2016**, *17*, 1224–1251.

- (26) Fang, C.; Tang, L.; Oscar, B. G.; Chen, C. Capturing Structural Snapshots during Photochemical Reactions with Ultrafast Raman Spectroscopy: From Materials Transformation to Biosensor Responses. *J. Phys. Chem. Lett.* **2018**, *9*, 3253–3263.
- (27) Wang, W.; Liu, W.; Chang, I.-Y.; Wills, L. A.; Zakharov, L. N.; Boettcher, S. W.; Cheong, P. H.-Y.; Fang, C.; Keszler, D. A. Electrolytic Synthesis of Aqueous Aluminum Nanoclusters and *in situ* Characterization by Femtosecond Raman Spectroscopy & Computations. *Proc. Natl. Acad. Sci. U. S. A.* **2013**, *110*, 18397-18401.
- (28) Stowers, J.; Anderson, J.; Cardineau, B.; Clark, B.; De Schepper, P.; Edson, J.; Greer, M.; Jiang, K.; Kocsis, M.; Meyers, S.; et al. "Metal Oxide EUV Photoresist Performance for N7 Relevant Patterns and Processes"; Proc. SPIE 9779, Advances in Patterning Materials and Processes XXXIII, 977904, 2016.
 - (29) Wrighton, M. The Photochemistry of Metal Carbonyls. Chem. Rev. 1974, 74, 401-430.
- (30) Pollak, C.; Rosa, A.; Baerends, E. J. Cr–CO Photodissociation in Cr(CO)₆: Reassessment of the Role of Ligand-Field Excited States in the Photochemical Dissociation of Metal–Ligand Bonds. *J. Am. Chem. Soc.* **1997**, *119*, 7324-7329.
- (31) Mendes, M.; Regeta, K.; Ferreira da Silva, F.; Jones, N. C.; Hoffmann, S. V.; García, G.; Daniel, C.; Limão-Vieira, P. Comprehensive Investigation of the Electronic Excitation of W(CO)₆ by Photoabsorption and Theoretical Analysis in the Energy Region from 3.9 to 10.8 eV. *Beilstein J. Nanotechnol.* **2017**, *8*, 2208-2218.
- (32) Meyer, T. J.; Caspar, J. V. Photochemistry of Metal-Metal Bonds. *Chem. Rev.* **1985**, 85, 187-218.
- (33) Zhang, J. Z.; Harris, C. B. Photodissociation Dynamics of Mn₂(CO)₁₀ in Solution on Ultrafast Time Scales. *J. Chem. Phys.* **1991**, *95*, 4024-4032.

- (34) Chen, J.; Zhang, H.; Tomov, I. V.; Ding, X.; Rentzepis, P. M. Photochemistry and Electron-transfer Mechanism of Transition Metal Oxalato Complexes Excited in the Charge Transfer Band. *Proc. Natl. Acad. Sci. U. S. A.* **2008**, *105*, 15235-15240.
- (35) Vogel, K. M.; Kozlowski, P. M.; Zgierski, M. Z.; Spiro, T. G. Role of the Axial Ligand in Heme–CO Backbonding; DFT Analysis of Vibrational Data. *Inorg. Chim. Acta* **2000**, *297*, 11-17.
- (36) Dougherty, T. P.; Heilweil, E. J. Ultrafast Transient Infrared Absorption Studies of M(CO)₆ (M = Cr, Mo or W) Photoproducts in *n*-Hexane Solution. *Chem. Phys. Lett.* **1994**, 227, 19-25.
- (37) Fang, C.; Tang, L.; Chen, C. Unveiling Coupled Electronic and Vibrational Motions of Chromophores in Condensed Phases. *J. Chem. Phys.* **2019**, *151*, 200901.
- (38) Scherer, J. R. Group Vibrations of Substituted Benzenes—I: E_{1u} Bend-stretch Modes and E_{2g} Ring Deformations of the Chlorobenzenes. *Spectrochim. Acta* **1963**, *19*, 601-610.
- (39) Liu, H. H.; Lin, S. H.; Yu, N. T. Resonance Raman Enhancement of Phenyl Ring Vibrational Modes in Phenyl Iron Complex of Myoglobin. *Biophys. J.* **1990**, *57*, 851-856.
- (40) Ketteringham, A. P.; Oldham, C. Raman Spectra of Multiply Bonded Metal Species. *J. Chem. Soc.*, *Dalton Trans.* **1973**, 1067-1070.
- (41) Fuß, W.; Trushin, S. A.; Schmid, W. E. Ultrafast Photochemistry of Metal Carbonyls. *Res. Chem. Intermed.* **2001**, *27*, 447-457.
- (42) Khudyakov, I.; Levin, P.; Kuzmin, V. Kinetics of Geminate Recombination of Organic Free Radicals in Viscous Solvents. *Photochem. Photobiol. Sci.* **2008**, *7*, 1540-1543.

- (43) Snellenburg, J. J.; Laptenok, S.; Seger, R.; Mullen, K. M.; van Stokkum, I. H. M. Glotaran: A Java-Based Graphical User Interface for the R Package TIMP. *J. Stat. Softw.* **2012**, *49*, 1-22.
- (44) Simon, J. D. Time-Resolved Studies of Solvation in Polar Media. *Acc. Chem. Res.* **1988**, *21*, 128-134.
- (45) Maroncelli, M.; Macinnis, J.; Fleming, G. R. Polar Solvent Dynamics and Electron-Transfer Reactions. *Science* **1989**, *243*, 1674.
- (46) Agmon, N.; Huppert, D.; Masad, A.; Pines, E. Excited-State Proton Transfer to Methanol-Water Mixtures. *J. Phys. Chem.* **1991**, *95*, 10407-10413.
- (47) Champness, N. R.; Levason, W. Coordination Chemistry of Stibine and Bismuthine Ligands. *Coord. Chem. Rev.* **1994**, *133*, 115-217.
- (48) Mitoraj, M. P.; Michalak, A. σ -Donor and π -Acceptor Properties of Phosphorus Ligands: An Insight from the Natural Orbitals for Chemical Valence. *Inorg. Chem.* **2010**, *49*, 578-582.
- (49) Burdett, J. K.; Grzybowski, J. M.; Perutz, R. N.; Poliakoff, M.; Turner, J. J.; Turner, R. F. Photolysis and Spectroscopy with Polarized Light: Key to the Photochemistry of Pentacarbonylchromium and Related Species. *Inorg. Chem.* **1978**, *17*, 147-154.
- (50) Ishikawa, Y.-i.; Kawakami, K. Structure and Infrared Spectroscopy of Group 6 Transition-Metal Carbonyls in the Gas Phase: DFT Studies on $M(CO)_n$ (M = Cr, Mo, and W; n = 6, 5, 4, and 3). *J. Phys. Chem. A* **2007**, *111*, 9940-9944.
- (51) Wang, L.; Zhu, X.; Spears, K. G. Unsaturated Transition-Metal Complexes in Solution: Naked Cr(CO)₅ in Cyclohexane Solution Observed by Picosecond IR Transient Absorption. *J. Am. Chem. Soc.* **1988**, *110*, 8695-8696.

- (52) Savéant, J.-M. Dissociative Electron Transfer. New Tests of the Theory in the Electrochemical and Homogeneous Reduction of Alkyl Halides. *J. Am. Chem. Soc.* **1992**, *114*, 10595-10602.
- (53) Matyushov, D. V. Solvent Reorganization Energy of Electron-Transfer Reactions in Polar Solvents. *J. Chem. Phys.* **2004**, *120*, 7532-7556.
- (54) Houmam, A. Electron Transfer Initiated Reactions: Bond Formation and Bond Dissociation. *Chem. Rev.* **2008**, *108*, 2180-2237.
- (55) Horng, M. L.; Gardecki, J. A.; Papazyan, A.; Maroncelli, M. Subpicosecond Measurements of Polar Solvation Dynamics: Coumarin 153 Revisited. *J. Phys. Chem.* **1995**, *99*, 17311-17337.
- (56) Toulson, B. W.; Borgwardt, M.; Wang, H.; Lackner, F.; Chatterley, A. S.; Pemmaraju, C. D.; Neumark, D. M.; Leone, S. R.; Prendergast, D.; Gessner, O. Probing Ultrafast C–Br Bond Fission in the UV Photochemistry of Bromoform with Core-to-valence Transient Absorption Spectroscopy. *Struct. Dyn.* **2019**, *6*, 054304.
- (57) Pérez-Lustres, J. L.; Rodriguez-Prieto, F.; Mosquera, M.; Senyushkina, T. A.; Ernsting, N. P.; Kovalenko, S. A. Ultrafast Proton Transfer to Solvent: Molecularity and Intermediates from Solvation- and Diffusion-Controlled Regimes. *J. Am. Chem. Soc.* **2007**, *129*, 5408-5418.
- (58) Reichardt, C.; Welton, T. Solvents and Solvent Effects in Organic Chemistry, 4th ed.; Wiley-VCH Verlag GmbH & Co. KGaA: Weinheim, Germany, 2011.
- (59) Chen, C.; Zhu, L.; Baranov, M. S.; Tang, L.; Baleeva, N. S.; Smirnov, A. Y.; Yampolsky, I. V.; Solntsev, K. M.; Fang, C. Photoinduced Proton Transfer of GFP-Inspired Fluorescent Superphotoacids: Principles and Design. *J. Phys. Chem. B* **2019**, *123*, 3804-3821.

- (60) Krueger, T. D.; Boulanger, S. A.; Zhu, L.; Tang, L.; Fang, C. Discovering a Rotational Barrier within a Charge-Transfer State of a Photoexcited Chromophore in Solution. *Struct. Dyn.* **2020**, *7*, 024901.
- (61) Xie, X.; Simon, J. D. Picosecond Time Resolved Absorption Studies of the Solvation of Cr(CO)₅ in Alcohols: A Unimolecular Kinetic Model for the Formation of Cr(CO)₅(OHR) from Photogenerated Cr(CO)₅(ROH). *J. Am. Chem. Soc.* **1990**, *112*, 1130-1136.
- (62) Zhang, Z.-F.; Su, M.-D. Mechanistic Study for the Photochemical Reactions of d⁶ M(CO)₅(CS) (M = Cr, Mo, and W) Complexes. *ACS Omega* **2017**, *2*, 2813-2826.
- (63) Karashima, S.; Yamamoto, Y.-i.; Suzuki, T. Ultrafast Internal Conversion and Solvation of Electrons in Water, Methanol, and Ethanol. *J. Phys. Chem. Lett.* **2019**, *10*, 4499-4504.
- (64) Tang, L.; Zhu, L.; Ener, M. E.; Gao, H.; Wang, Y.; Groves, J. T.; Spiro, T. G.; Fang, C. Photoinduced Charge Flow Inside an Iron Porphyrazine Complex. *Chem. Commun.* **2019**, *55*, 13606-13609.

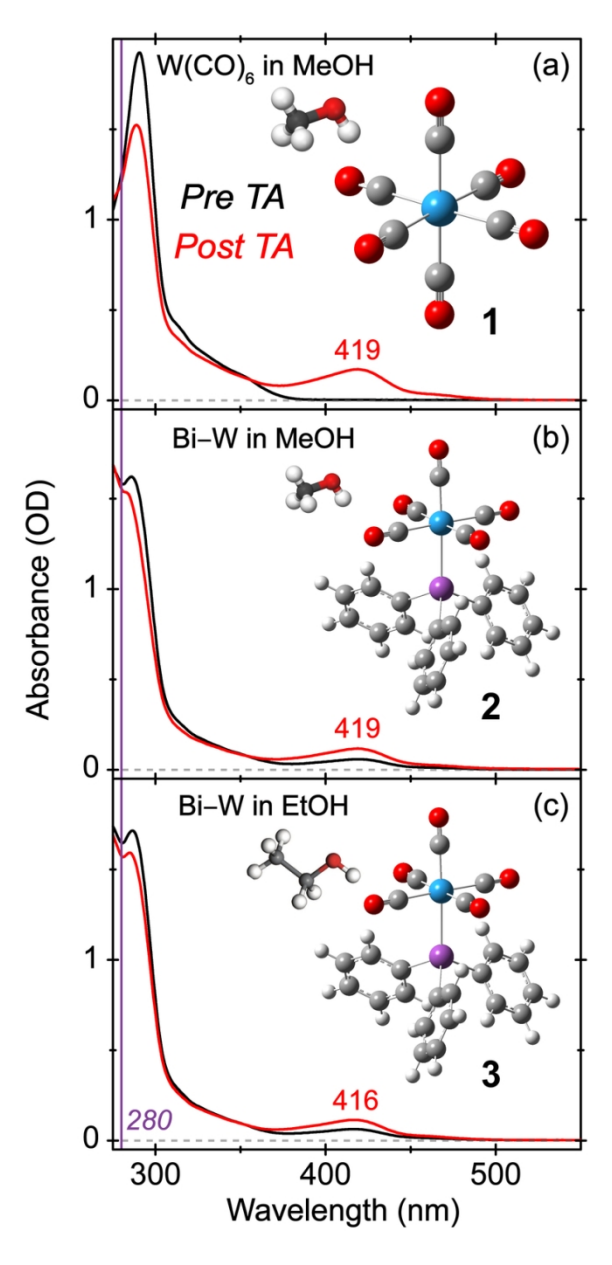


Figure 1. Chemical structures and steady-state electronic spectroscopy before (black) and after (red) UV photoexcitation of 2 mM (a) W(CO)₆ in MeOH, (b) Bi–W in MeOH, and (c) Bi–W in EtOH.

65x137mm (300 x 300 DPI)

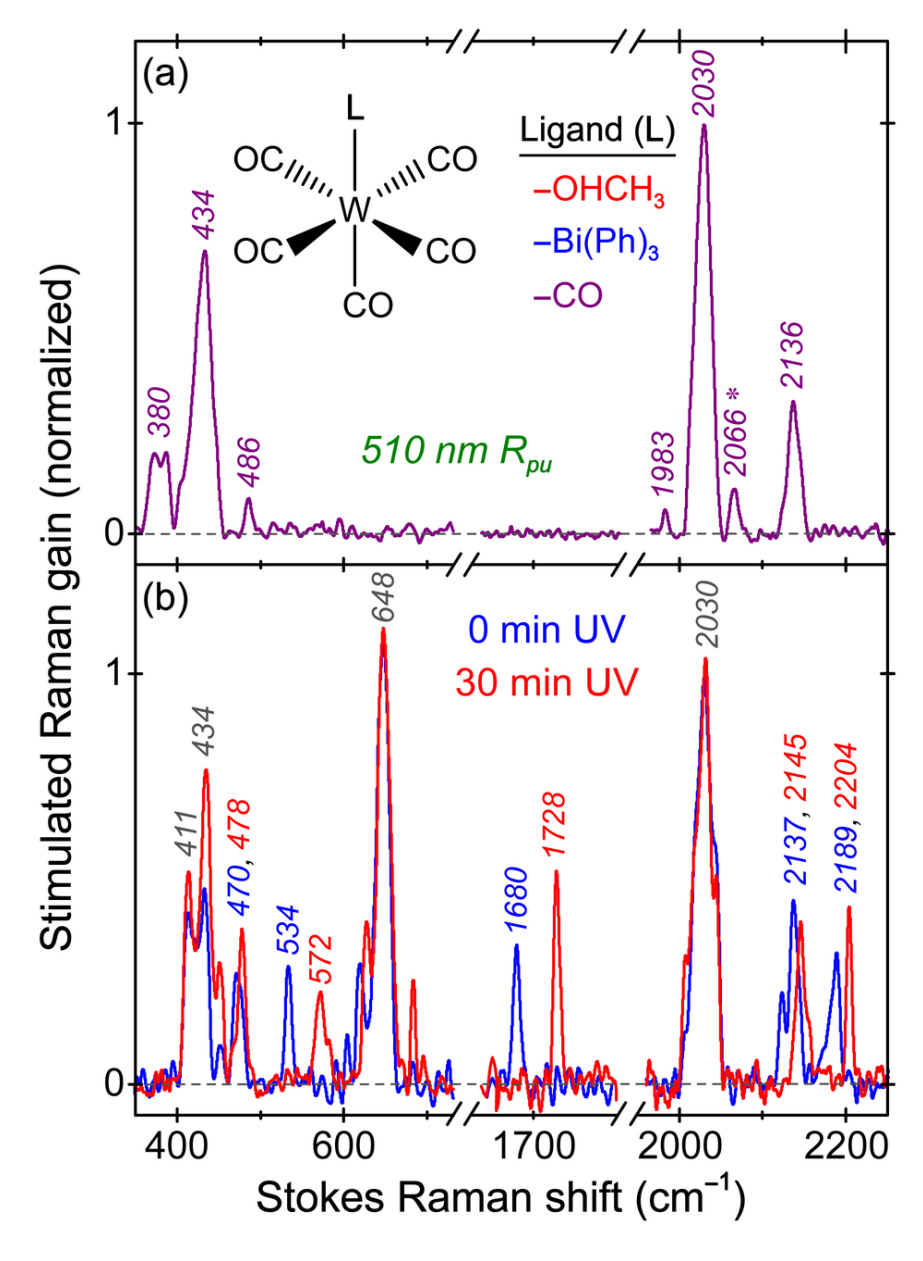


Figure 2. Normalized GS-FSRS spectra of 5 mM (a) $W(CO)_6$ in MeOH (purple) and (b) Bi–W in MeOH before (blue) and after (red) UV lamp irradiation at 254 nm for 30 minutes.

79x109mm (300 x 300 DPI)

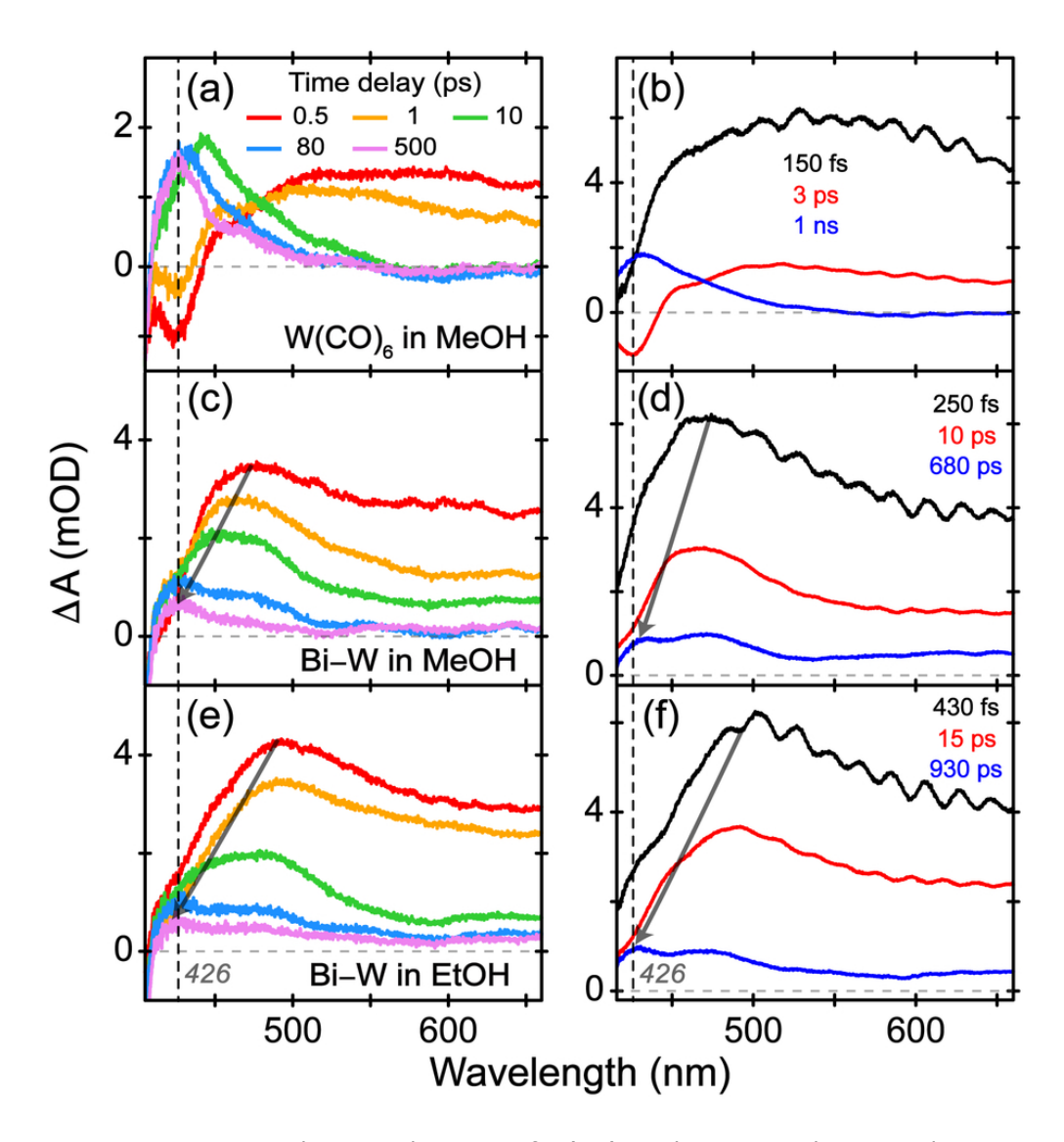


Figure 3. Transient electronic dynamics of W(CO) $_6$ and Bi–W complexes in solution. 78x84mm~(300~x~300~DPI)

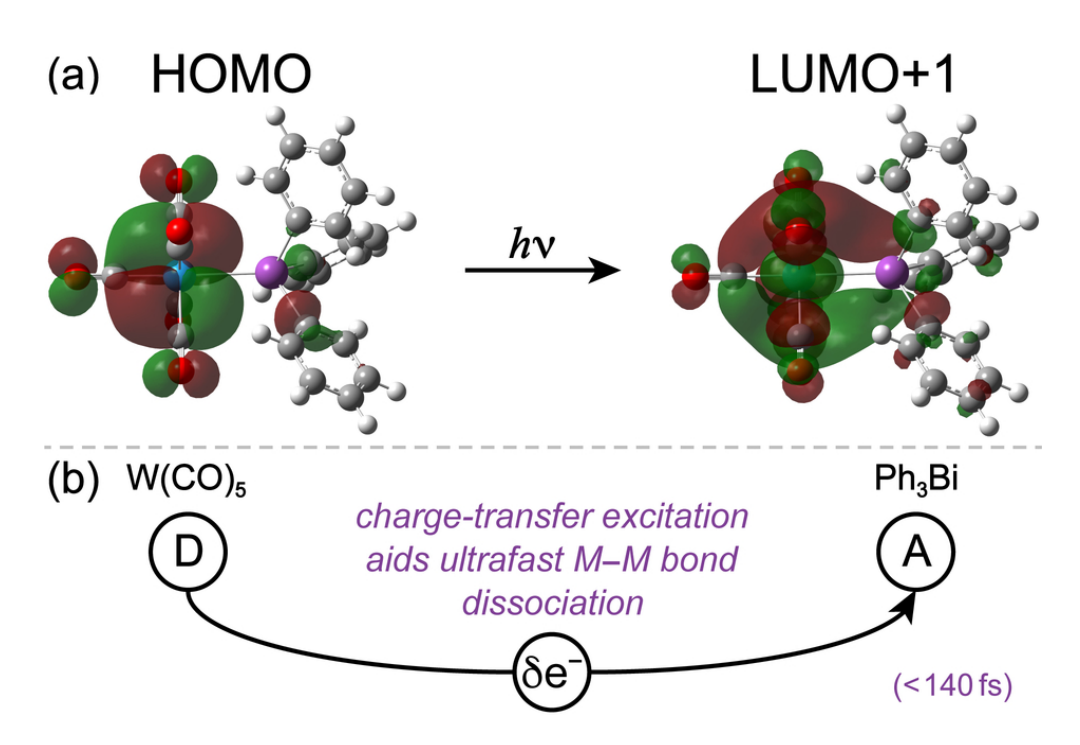
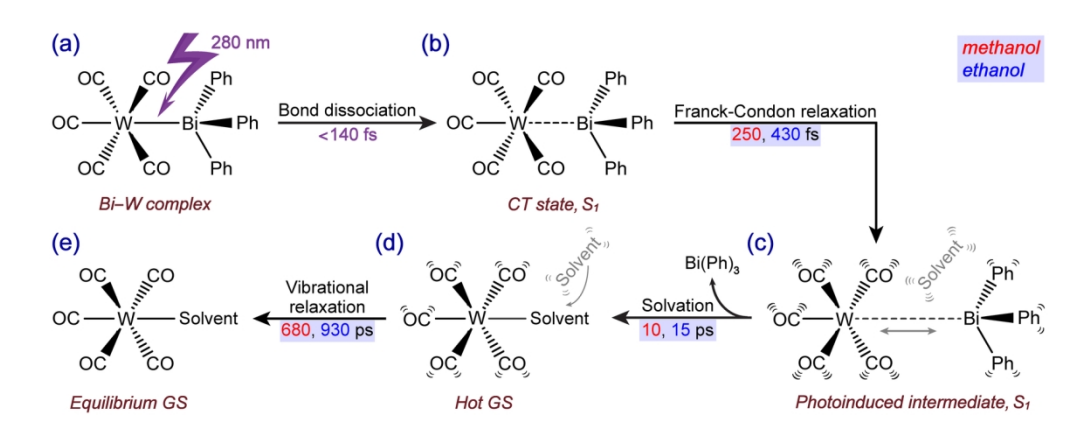
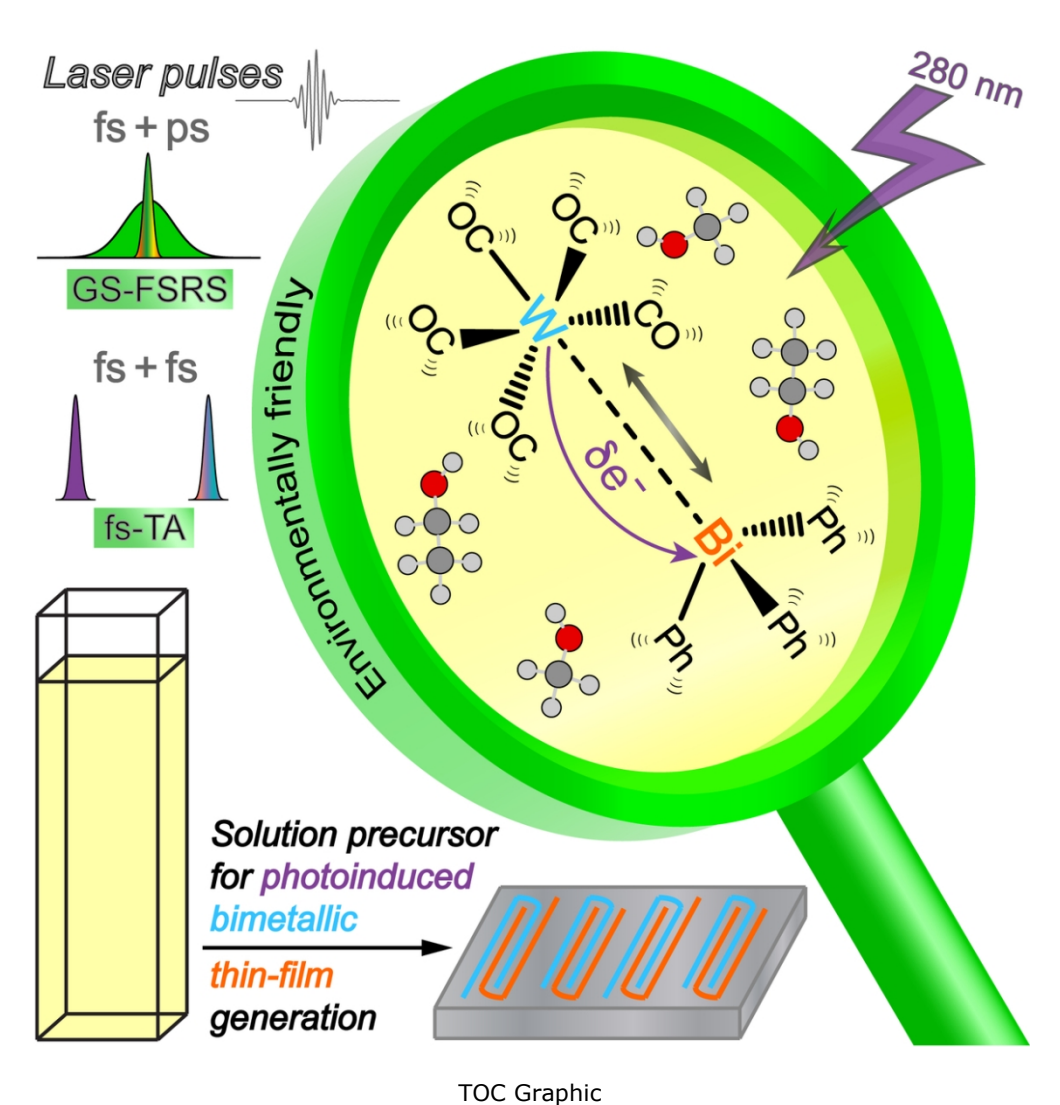


Figure 4. Quantum calculations imply the nature of electronic excitation. $80x53mm \; (300 \; x \; 300 \; DPI)$



Scheme 1. Photochemical reaction mechanism of Bi–W in solution. Characteristic time constants are listed by major steps converting the reactant (a) via intermediates to the product (e).

150x57mm (300 x 300 DPI)



49x49mm (600 x 600 DPI)